Applied Catalysis B: Environmental 152–153 (2014) 289–299

Contents lists available at ScienceDirect

Applied Catalysis B: Environmental

journal homepage: www.elsevier.com/locate/apcatb

Converting mixed plastics into mesoporous hollow carbon spheres with controllable diameter

Jiang Gong[a,b], Jie Liu[a], Zhiwei Jiang[a,b], Xuecheng Chen[a,c], Xin Wen[a], Ewa Mijowska[c], Tao Tang[a,*]

[a] State Key Laboratory of Polymer Physics and Chemistry, Changchun Institute of Applied Chemistry, Chinese Academy of Sciences, Changchun 130022, China
[b] University of Chinese Academy of Sciences, Beijing 100049, China
[c] Institute of Chemical and Environment Engineering, West Pomeranian University of Technology, Szczecinul. Pulaskiego 10, 70-322 Szczecin, Poland

ARTICLE INFO

Article history:
Received 22 December 2013
Received in revised form 14 January 2014
Accepted 24 January 2014
Available online 2 February 2014

Keywords:
Mixed plastics
Co_3O_4
Organically modified montmorillonite
Hollow carbon sphere
Combined catalysis

ABSTRACT

Upcycling waste plastics into high value-added carbon nanomaterials has been a hot topic due to ever-increasing generation of waste plastics, however, little attention has been paid to valuable hollow carbon spheres (HCSs). Herein, uniform mesoporous HCSs with controllable diameter and high surface area were efficiently prepared through the carbonization of mixed plastics consisting of polypropylene, polyethylene and polystyrene under the combined catalysis of organically-modified montmorillonite (OMMT)/Co_3O_4 at 700 °C. The morphology, microstructure, phase structure, textural property, surface element composition and thermal stability of HCSs were investigated by scanning electron microscope, transmission electron microscope (TEM), high-resolution TEM, X-ray diffraction, Raman spectroscopy, N_2 sorption, X-ray photoelectron spectroscopy and thermal gravimetric analysis. The effects of OMMT on the dispersion of Co_3O_4 in the mixed plastics and the degradation of mixed plastics were studied. It was found that OMMT not only promoted the dispersion of Co_3O_4 in the mixed plastics, which favored to control the diameter of HCSs, but also promoted the degradation of mixed plastics into light hydrocarbons and aromatics, which facilitated the growth of HCSs. Finally, a possible mechanism was proposed to explain the growth of uniform HCSs with controllable diameter. This facile method provides a novel potential way to convert waste plastics into valuable HCSs, which can be used as catalyst support, adsorbent, storage medium and template for the synthesis of other useful hollow materials, etc.

1. Introduction

Considerable attention has been paid to the treatment of waste plastics with ever-growing production and consumption of plastics since they are not biodegradation [1–3]. Landfill and incineration are far from being widely accepted due to their related environmental pollution. Upcycling is the process of converting waste materials into something useful and more valuable. Chemical recycling can recover the petrochemical components of waste plastics, which could be used to produce other synthetic chemicals [4–7]. Anyhow, great efforts have been made to explore a new technically and economically feasible chemical recycling process for the treatment of waste plastics.

Up to now, many studies [8–23] have been conducted on converting virgin or waste plastics including polypropylene (PP), polyethylene (PE) and polystyrene (PS) into high value-added carbon nanomaterials (CNMs) with diverse morphologies and microstructures such as carbon nanotubes (CNTs), cup-stacked CNTs (CS-CNTs) and carbon nanofibers (CNFs). For example, Wu et al. used catalytic gasification to process waste plastics into CNTs and hydrogen-rich synthetic gas by using Ni/Ca-Al or Ni/Zn-Al catalyst [8,9]. Acomb et al. used pyrolysis–gasification of PP, PE and PS to prepare CNTs and hydrogen by Ni/Al_2O_3 catalyst [10]. Zhuo et al. reported the synthesis of CNTs and CNFs from recycled PE using stainless-steel wire mesh as catalyst by a novel pyrolysis–combustion technique [11–13]. Pol et al. used autoclave as reactor to convert waste PE into CNTs using $Co(Ac)_2$ as catalyst under high pressure [14]. Our group put forward a strategy of combined degradation catalyst/carbonization catalyst, including solid acid (such as organically modified montmorillonite (OMMT) or zeolite)/nickel catalyst [15–19], halogenated compound/Ni_2O_3

* Corresponding author. Tel.: +86 431 85262004; fax: +86 431 85262827.
E-mail address: ttang@ciac.ac.cn (T. Tang).

0926-3373/$ – see front matter © 2014 Elsevier B.V. All rights reserved.
http://dx.doi.org/10.1016/j.apcatb.2014.01.051

[20–22] and activated carbon/Ni_2O_3 [23], to effectively convert PP and PE into CNTs, CS-CNTs and CNFs under atmospheric condition.

However, most of current studies are limited to focusing on single component plastic, and there are few studies attempting to transform mixed plastics into CNMs. This is essential to effectively convert waste plastics into CNMs because the "real-world" waste plastic is actually mixture which mainly consists of PP, PE and PS [24]. In addition, although CNMs with diverse morphologies and microstructures have been prepared using plastics as carbon sources [8–23], to the best of our knowledge, little attention has been paid to hollow carbon spheres (HCSs). HCSs with a structure of hollow core and carbon shell have attracted great interests due to their unique physicochemical properties, such as low density, large inner space and specific surface area, and wide applications in catalyst support, adsorbent, storage medium and template for the synthesis of other useful hollow materials [25–34].

So far, there have been only two reports about synthesizing HCSs using plastics as carbon sources. Chen et al. prepared HCSs using PP as carbon source and the combined OMMT/$Co(Ac)_2$ as catalyst [35]. But the obtained HCSs showed extreme heterogeneity in the size distribution and the yield of HCSs was just 9 wt%. In our previous report [36], uniform HCSs were prepared through the carbonization of PS under the catalysis of OMMT/cobalt catalyst (including Co_2O_3, Co_3O_4 and $Co(AC)_2$). It was found that OMMT promoted the degradation of PS into light hydrocarbons and aromatics, while cobalt catalyst acted as template for the growth of HCSs by carbonizing light hydrocarbons and aromatics. However, the yield of HCSs was less than 15 wt%, and the diameter of HCSs could not be controlled. The previous work prompted us to raise further questions: How does the content of cobalt catalyst influence the yield and diameter of HCSs using mixed plastics as carbon sources? How does OMMT affect the degradation products of mixed plastics? Solving these problems will not only provide more insights into the carbonization mechanism of mixed plastics, but also contribute to converting waste plastics into high value-added HCSs.

Herein, firstly, uniform mesoporous HCSs with controllable diameter and high surface area were effectively prepared through the carbonization of mixed plastics consisting of PP, PE and PS under the catalysis of OMMT/Co_3O_4 at 700 °C. The effects of Co_3O_4 content on the yield, morphology, phase structure, textural property, surface element composition and thermal stability of HCSs were investigated. Subsequently, the effects of OMMT on the dispersion of Co_3O_4 in the mixed plastics and the degradation of mixed plastics were studied. Finally, a possible mechanism was proposed to explain the growth of uniform HCSs with controllable diameter using mixed plastics as carbon sources. This simple method provides a novel potential way to convert waste plastics into high value-added HCSs.

2. Experimental part

2.1. Materials

Polypropylene (PP) powder was supplied by Yanan Petrochemical Co., China. High density polyethylene (PE) pellet was obtained from Sinopec Yangzi Petrochemical Co., Ltd. Polystyrene (PS) pellet was supplied by Zhenjiang Qimei Chemical Co., Ltd., China. Co_3O_4 was analytical-grade quality and purchased from Sinopharm Chemical Reagents Co., Ltd., China. OMMT (Closite 15A, organic modifier: dimethyl-dihydrogenated tallow quarternary ammonium; modifier concentration: 125 mequiv per 100 g clay) was purchased from Southern Clay. All other chemicals were of analytical-grade quality.

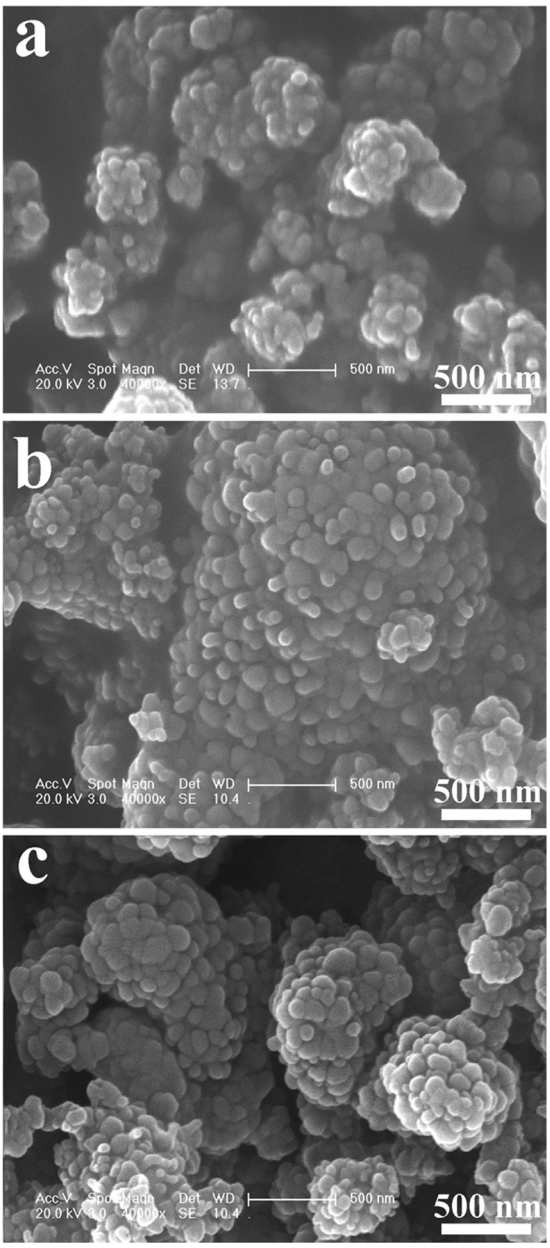

Fig. 1. Typical SEM images of HCSs from polymer/OMMT-Co_3O_4: (a) HCS-10, (b) HCS-30 and (c) HCS-50.

2.2. Preparation of samples

Mixed plastics consisting of PP (26.9 wt%, 9.42 g), PE (56.3 wt%, 19.70 g) and PS (16.8 wt%, 5.88 g) were mixed with OMMT (5.25 g) and a designed amount of Co_3O_4 in a Brabender mixer at 100 rpm and 180 °C for 10 min. The resultant sample was designed as polymer/OMMT-Co_3O_4-x, where polymer and x represented the "mixed plastics" and the content of Co_3O_4 (g/100 g polymer), respectively. For comparison, polymer/OMMT with OMMT content of 15 (g/100 g polymer) and polymer/Co_3O_4-x were also prepared.

2.3. Preparation of HCSs

HCSs were prepared through carbonization experiment by heating polymer/OMMT-Co_3O_4-x in a crucible at 700 °C according to our previous report [20]. Briefly, a piece of polymer/OMMT-Co_3O_4-x (about 11.0 g) was placed into a crucible, which was heated at 700 °C for about 8 min. Subsequently, the charred residue in the

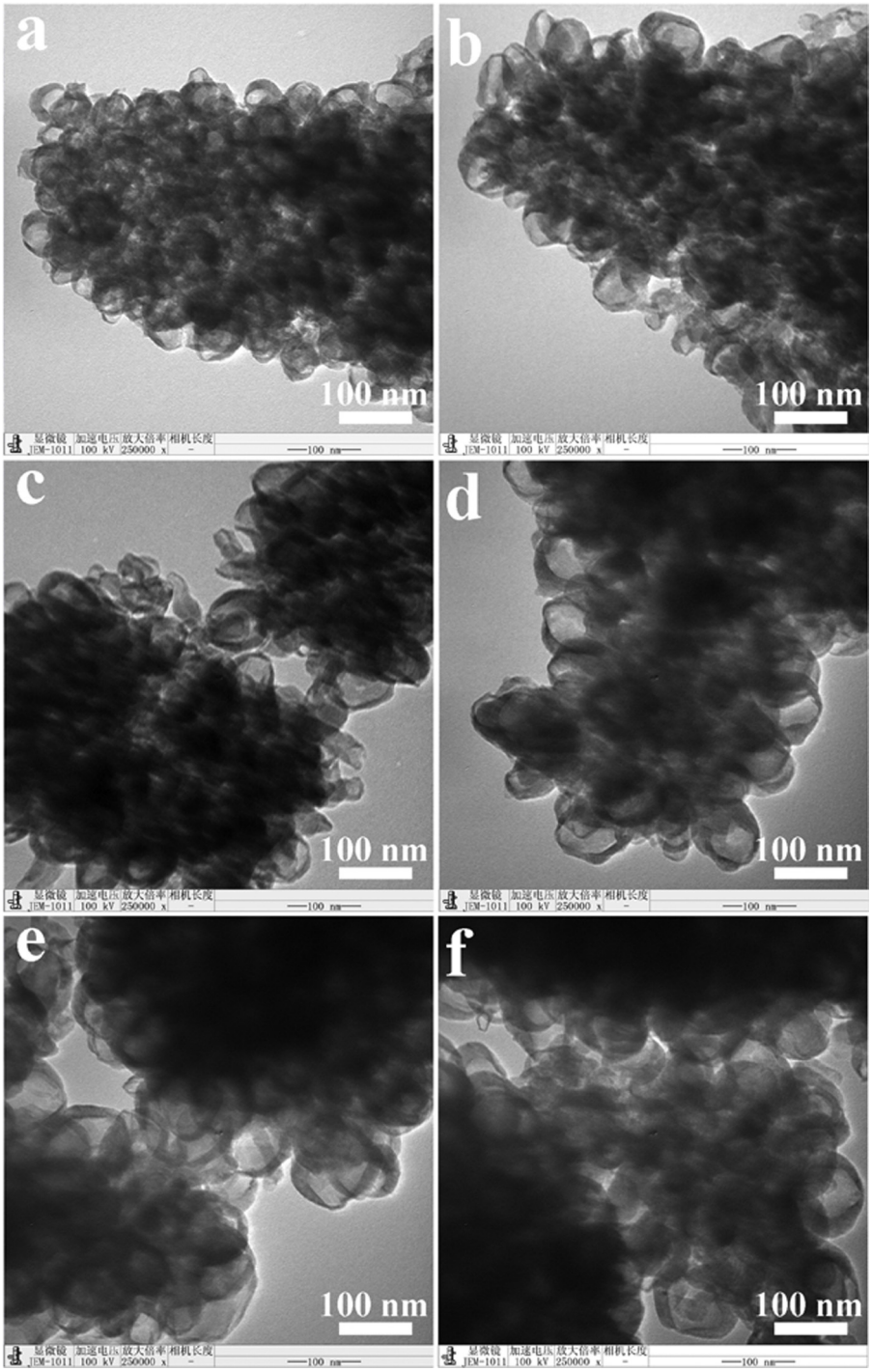

Fig. 2. Typical TEM images of HCSs from polymer/OMMT-Co_3O_4: (a) HCS-10, (b) HCS-20, (c) HCS-30, (d) HCS-40, (e) HCS-50 and (f) HCS-60.

crucible was purified with hydrofluoric acid and nitric acid to eliminate montmorillonite (MMT), amorphous carbon and cobalt catalyst. The resultant HCSs were designated as HCS-x, where x represented the content of Co_3O_4 in the polymer/OMMT-Co_3O_4-x. The yield of HCSs was calculated by dividing the amount of purified carbon product by that of carbon element in the mixed plastics from the sample. Each measurement was repeated four times for the purpose of reproducibility.

The degradation products of mixed plastics are carbon feedstock for the formation of HCSs. To study the effect of OMMT on the degradation products of mixed plastics, pyrolysis experiments [20] for mixed plastics and polymer/OMMT were conducted at 700 °C. The liquid pyrolyzed products were collected using a cold trap and the gas pyrolyzed products were collected using a sample bag.

2.4. Characterization

The morphology of HCSs was observed by field-emission scanning electron microscope (SEM, XL30ESEM-FEG). The microstructure of HCSs was investigated using transmission electron microscope (TEM, JEM-1011) at an accelerating voltage of 100 kV and high-resolution TEM (HRTEM) on a FEI Tecnai G2 S-Twin transmission electron microscope operating at 200 kV. The phase structures of the charred residues before purification, HCSs and

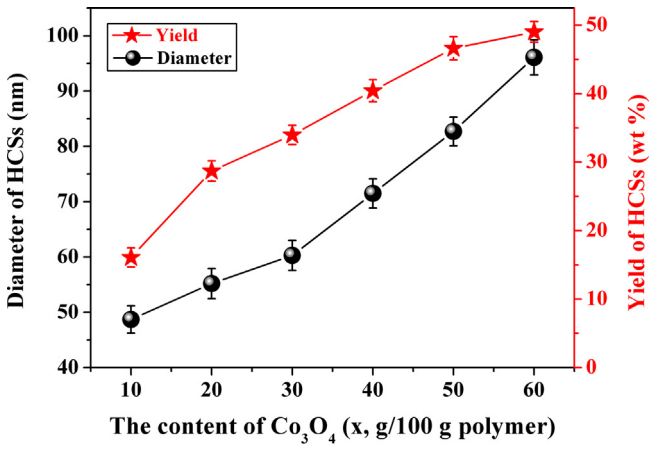

Fig. 3. Effects of Co_3O_4 content on the diameter (calculated according to TEM results) and yield of HCSs from polymer/OMMT-Co_3O_4.

mixed plastics were analyzed by X-ray diffraction (XRD) using a D8 advance X-ray diffractometer with Cu Kα radiation operating at 40 kV and 200 mA. Raman spectroscopy (T6400, excitation-beam wavelength: 514.5 nm) was used to characterize the vibrational property of HCSs. The textural property of HCSs was measured by N_2 sorption at 77 K using a Quantachrome Autosorb-1C-MS analyzer. The specific surface area was calculated by BET method, and the contribution of micropores to both volume and surface area was evaluated by means of the *t*-plot method. The surface element composition of HCSs was characterized by means of X-ray photoelectron spectroscopy (XPS) carried out on a VG ESCALAB MK II spectrometer using an Al Kα exciting radiation from an X-ray source operated at 10.0 kV and 10 mA. The thermal stability of HCSs was measured by thermal gravimetric analysis (TGA) under air flow at a heating rate of 10 °C/min using a TA Instruments SDT Q600. The microstructure of the charred residues before purification was investigated using TEM (JEM-1011) at an accelerating voltage of 100 kV.

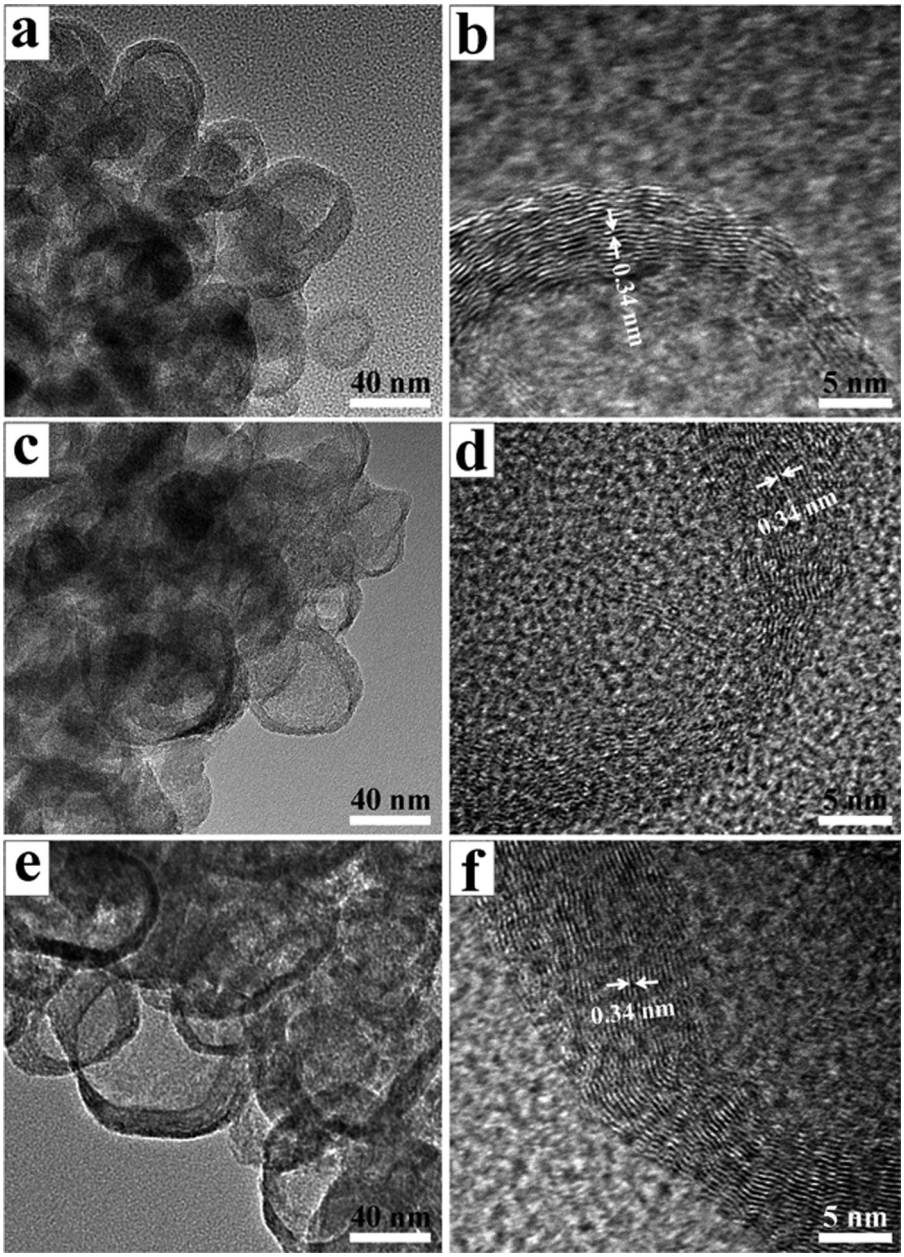

Fig. 4. HRTEM images of HCSs from polymer/OMMT-Co_3O_4: (a and b) HCS-10, (c and d) HCS-30, and (e and f) HCS-60.

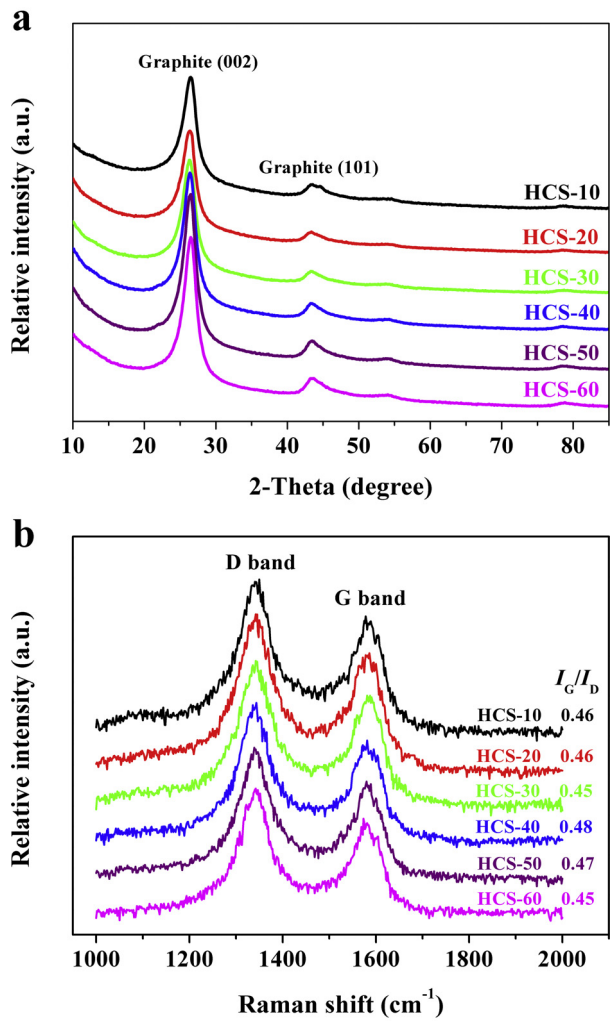

Fig. 5. XRD patterns (a) and Raman spectra (b) of HCSs.

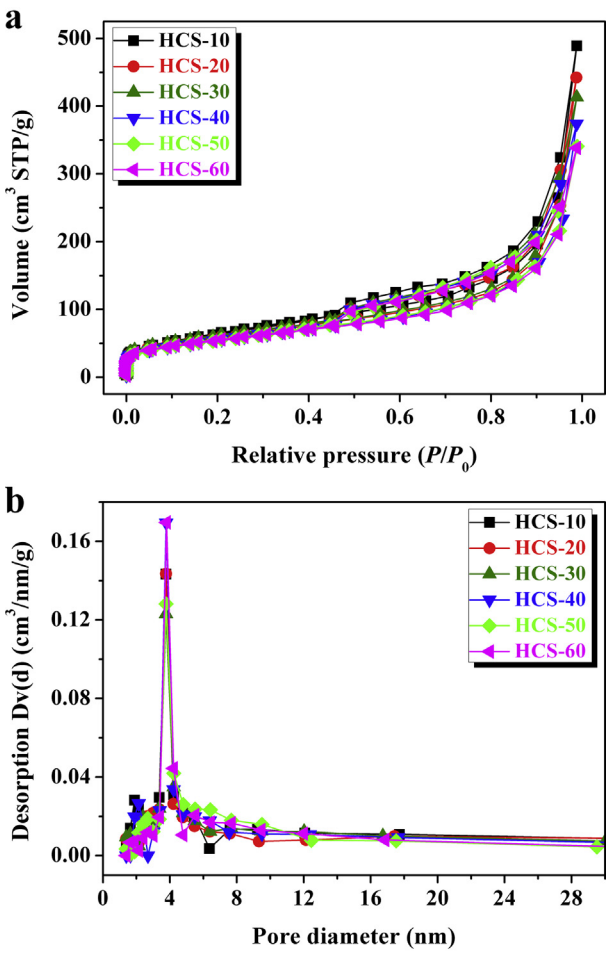

Fig. 6. Nitrogen adsorption–desorption isotherms (a) and pore size distributions (b) of HCSs.

Table 1
Textural parameters of HCSs.

Property	HCS-10	HCS-20	HCS-30	HCS-40	HCS-50	HCS-60
S_{BET} (m^2/g)[a]	238.7	210.2	218.6	195.2	196.6	196.0
S_{micro} (m^2/g)[b]	15.9	19.9	38.5	9.3	7.5	29.4
S_{meso} (m^2/g)[c]	222.8	190.3	180.1	185.9	189.1	166.6
V_{total} (cm^3/g)[d]	0.757	0.684	0.639	0.579	0.527	0.524
V_{micro} (cm^3/g)[e]	0.004	0.005	0.018	0.004	0.003	0.013
V_{meso} (cm^3/g)[f]	0.753	0.679	0.621	0.575	0.524	0.511
D_{AV} (nm)[g]	3.77	3.77	3.77	3.78	3.78	3.80

[a] The total specific surface area.
[b] The specific surface area of micropores.
[c] The specific surface area of mesopores.
[d] The total volume of pores.
[e] The volume of micropores.
[f] The volume of mesopores.
[g] The average diameter of pores.

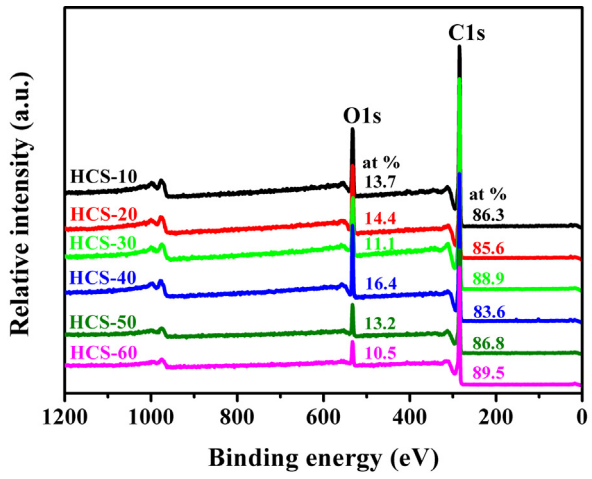

Fig. 7. XPS patterns of HCSs.

The rheological properties of mixed plastics and its mixture were conducted on a controlled strain rate rheometer (ARES rheometer) under nitrogen atmosphere. Round samples 25 mm (diameter) × 1 mm (thickness) were run at 180 °C. Frequency sweep was performed from 0.01 to 100 rad/s, with a strain of 1% in order to make the materials be in linear viscoelastic response. The morphologies of mixed plastics and its mixture were observed by means of SEM (XL30ESEM-FEG). To study the effect of OMMT on the degradation products of mixed plastics, the collected liquid products were weighed and analyzed by gas chromatography-mass spectrometry (GC–MS, AGILENT 5975MSD). The volume of collected gas products was determined by the displacement of water. The hydrocarbon gas products were analyzed by a GC (Kechuang, GC 9800) equipped with a FID, using a KB-Al_2O_3/Na_2SO_4 column (50 m × 0.53 mm i.d.). H_2, CO and CH_4 were analyzed by a GC (Kechuang, GC 9800) equipped with a TCD, using a packed TDX-01 (1 m) and molecular sieve 5 Å column (1.5 m).

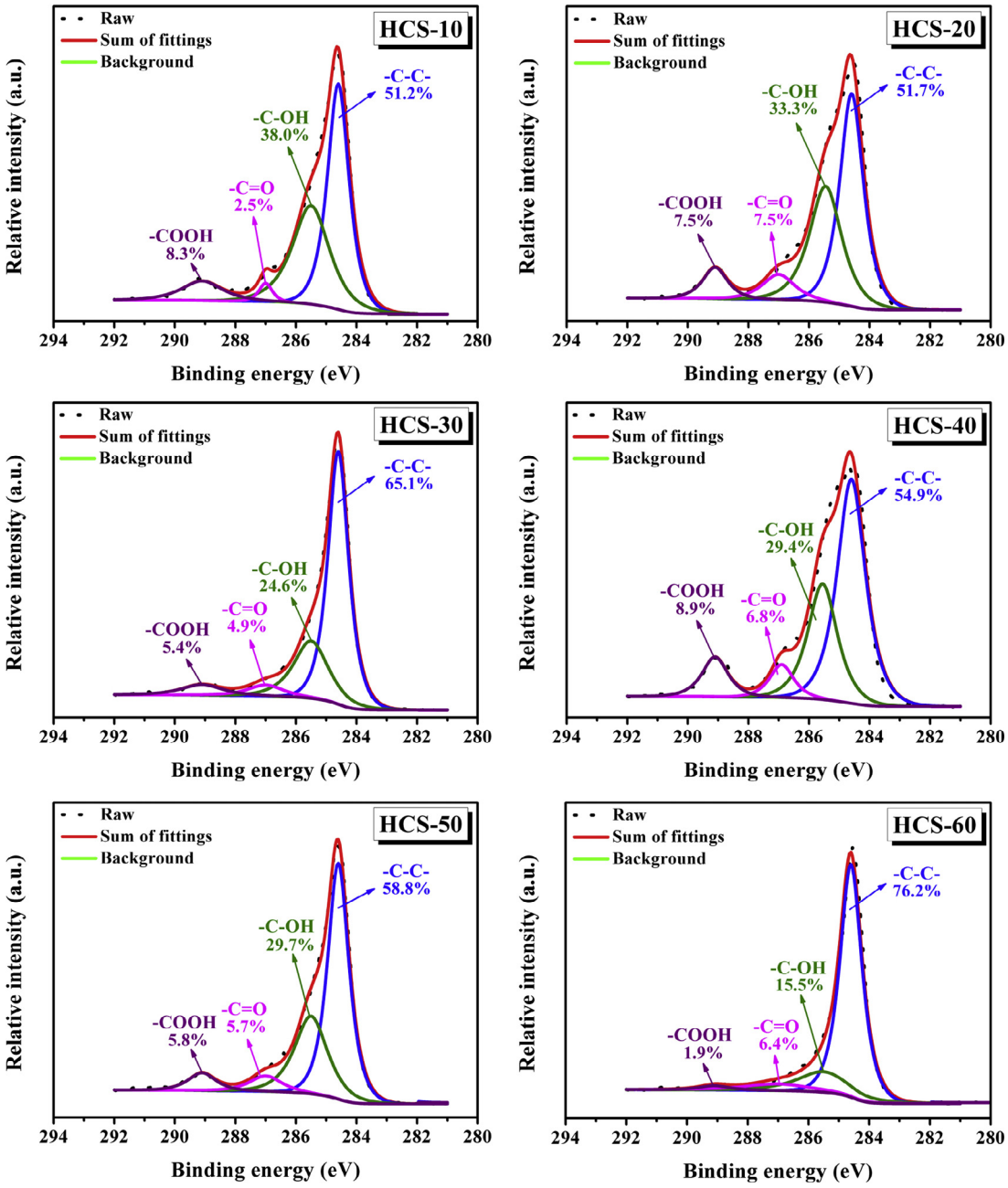

Fig. 8. C1s high-resolution XPS spectra of HCSs.

3. Result and discussion

3.1. Morphology, microstructure and yield of HCSs

To study the effect of Co_3O_4 content on the morphology of HCSs, SEM observation was conducted. Fig. 1 and S1 (in the supporting information) show SEM images of the resultant HCSs from polymer/OMMT-Co_3O_4 with different contents of Co_3O_4. Clearly, a great amount of aggregated spherical-shape nanoparticles with dozens of nanometers were observed in the resultant HCSs. When the content of Co_3O_4 was increased, the size of nanospheres became larger. To gain more detailed information about the internal microstructure of HCSs, TEM and HRTEM observations were conducted. TEM images of the HCSs (Fig. 2) demonstrated that they were comprised of uniform carbon nanospheres with central hollow inside. The diameter distribution histograms of HCSs are displayed in Fig. S2, and the average diameters of HCSs are shown in Fig. 3. The average diameter was 48.7 nm for HCS-10, 55.2 nm for HCS-20, 60.3 nm for HCS-30, 71.5 nm for HCS-40, 82.7 nm for HCS-50, and 96.1 nm for HCS-60. Hence, it was demonstrated that the diameter of HCSs could be controlled by adjusting the content of Co_3O_4. HRTEM images of the HCSs are shown in Fig. 4, further revealing the microstructure of hollow carbon spheres. The carbon shell had an ordered and curved graphitic structure. Furthermore, the interlayer spacing between graphitic layers was in the range of 0.33–0.35 nm, consistent with the ideal graphitic interlayer spacing. The thicknesses of the graphitic shells fell in the range of 4–16 nm.

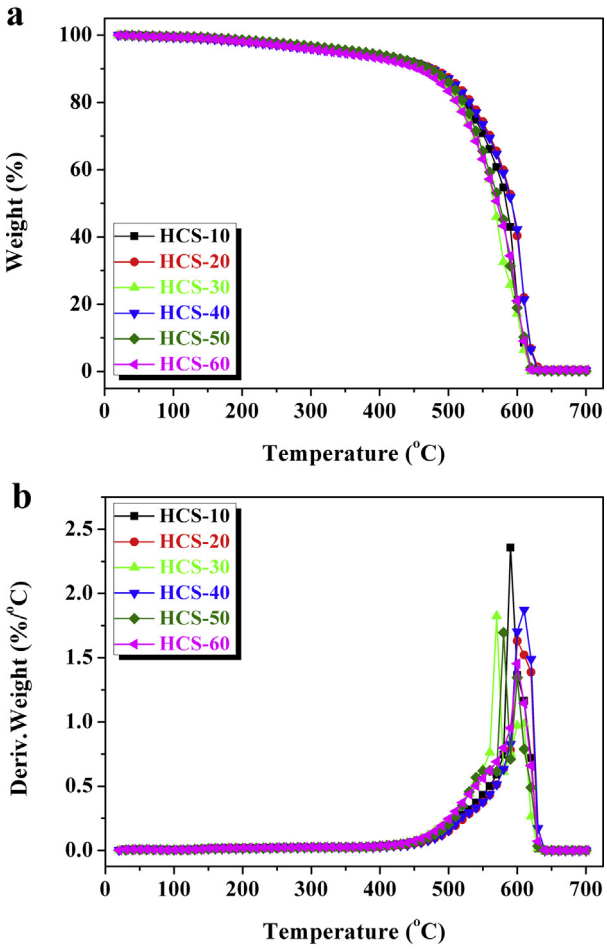

Fig. 9. TGA (a) and DTG (b) curves of HCSs under air flow at 10 °C/min.

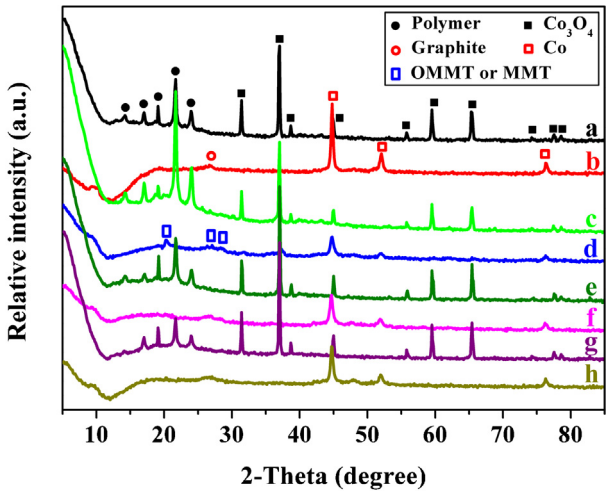

Fig. 10. XRD patterns of polymer/Co_3O_4-30 (a) and its carbonized product before purification (b), and polymer/OMMT-Co_3O_4 (polymer/OMMT-Co_3O_4-10 (c), polymer/OMMT-Co_3O_4-30 (e) and polymer/OMMT-Co_3O_4-60 (g)) and their carbonized products before purification (Co@C-10 (d), Co@C-30 (f) and Co@C-60 (h)).

The yields of HCSs from polymer/OMMT-Co_3O_4 with different contents of Co_3O_4 are shown in Fig. 3. As can be seen, when the content of Co_3O_4 was increased from 10 to 60 (g/100 g polymer), the yield of HCSs increased from 10.1 to 49.0 wt%, indicating that Co_3O_4 catalyst played an important role in the formation of HCSs. The yield of carbon products from polymer/Co_3O_4-60 and polymer/OMMT was 26.7 and 1.1 wt%, respectively, much lower than that from polymer/OMMT-Co_3O_4-60 (i.e., 49.0 wt%), suggesting that the combined OMMT/Co_3O_4 showed a synergetic effect on the carbonization of mixed plastics into HCSs. More investigations about the roles of OMMT and Co_3O_4 on the catalytic carbonization of mixed plastics into HCSs were conducted in Section 3.3.

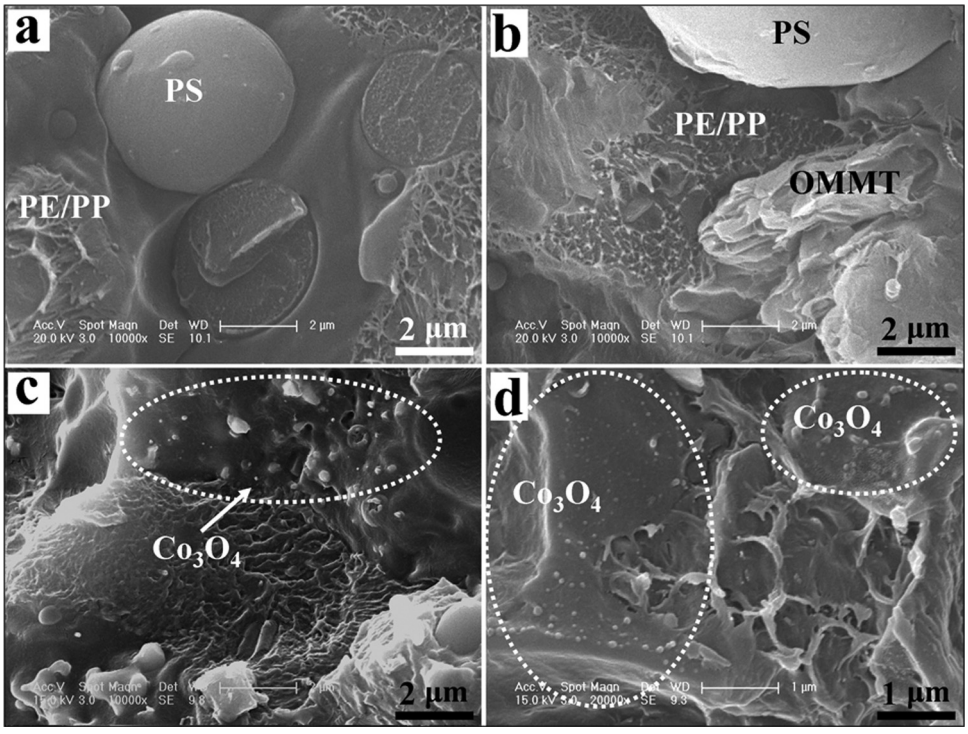

Fig. 11. Typical SEM images of polymer (i.e., mixed plastics) (a), polymer/OMMT (b), polymer/Co_3O_4-10 (c) and polymer/OMMT-Co_3O_4-10 (d).

3.2. Phase structure, textural property, surface element composition and thermal stability of HCSs

The graphitization degree of the resultant HCSs was characterized by XRD and Raman spectroscopy. Fig. 5a displays the XRD patterns of HCSs. The two diffraction peaks at about 26.5° and 43.3° were assigned to the typical graphitic (0 0 2) and (1 0 1) planes, respectively. The sharp and strong graphite (0 0 2) diffraction peak of the HCSs indicated the high degree of graphitization of HCSs. No diffraction peaks of metallic cobalt or OMMT were detected in the obtained HCSs, implying that the remained metallic cobalt catalyst and OMMT were removed after the purification. Fig. 5b shows the Raman spectra of HCSs. The peak at about 1580 cm^{-1} (G band) corresponds to an E_{2g} mode of hexagonal graphite and is related to the vibration of sp^2-bonded carbon atoms in a graphite layer. This meant that HCSs were composed of graphitic carbon, consistent with HRTEM and XRD results. The D band at about 1350 cm^{-1} is associated with the vibration of carbon atoms with dangling bonds in the plane terminations of disordered graphite. The intensity ratio of G band and D band (I_G/I_D ratio) provides information about the crystallinity of HCSs [37]. The I_G/I_D ratios of HCSs were in the range of 0.45–0.48, reflecting the presence of a relative high amount of disordered carbon in the HCSs.

The nitrogen adsorption–desorption isotherms of the obtained HCSs (Fig. 6a) showed the type-IV curve and exhibited a hysteresis loop associated to capillary condensation in the range of P/P_0 being from 0.5 to 1.0. This indicated that the porosity of the obtained HCSs was essentially made up of mesopores. The textural properties of HCSs, including BET surface area (S_{BET}), micropore surface area (S_{micro}), mesopore surface area (S_{meso}), total pore volume (V_{total}), micropore volume (V_{micro}), mesopore volume (V_{meso}) and average pore diameter (D_{AV}), are summarized in Table 1. S_{BET}, S_{meso}, V_{total} and V_{meso} of HCSs were in the range of 196–238.7 m^2/g, 166.6–222.8 m^2/g, 0.524–0.757 cm^3/g and 0.511–0.753 cm^3/g, respectively. The pore size distributions of HCSs were calculated using the Barrett–Joyner–Halenda (BJH) model from the desorption branches of the isotherms (Fig. 6b). This clearly showed that the size of mesopores in the HCSs was in the narrow range of 2–5 nm (centered on 3.8 nm). The mesopores could be attributed to the cavities in the HCSs.

XPS measurement was used to characterize the surface element composition of the mesoporous HCSs. It revealed that the surface of mesoporous HCSs mainly consisted of C and O elements, with no evidence of any other elements (Fig. 7). To determine the chemical component and the oxidation state of C element, high-resolution XPS spectra of C_{1s} were curve-fitted into four individual peaks: graphitic carbon (284.4–284.6 eV), C–OH (285.6–285.8 eV), C=O (286.9–287.1 eV) and COOH (288.9–289.1 eV) (Fig. 8). These results indicated that the carbon element on the surface of the mesoporous HCSs existed in the presence of graphitic carbon with relatively small amounts of C–OH, C=O and COOH. These surface functional groups could contribute to the removal of heavy metallic ions [38] or organic dyes [39] when the mesoporous HCSs were used as adsorbents in wastewater treatment.

TGA and the derivative TGA (DTG) were used to evaluate the graphitic nature and the purity of HCSs (Fig. 9). The weight loss of HCSs showed three stages. The weight loss before 100 °C was due to the evaporation of physically adsorbed water molecules in HCSs. The second weak region of weight loss from 100 to 400 °C was attributed to the release of chemisorbed water and the pyrolysis of oxygen containing functional groups in the HCSs. A remarkable weight loss occurred in the range of 400–700 °C, which was ascribed to the oxidation of carbon skeleton of graphite shells. The residues of HCSs at 700 °C were less than 0.3%, demonstrating that the HCSs had a high purity.

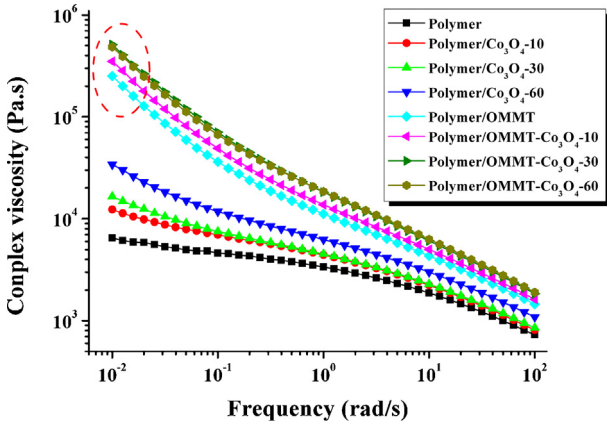

Fig. 12. Complex viscosity of polymer, polymer/Co_3O_4, polymer/OMMT and polymer/OMMT-Co_3O_4.

3.3. Discussion about the growth mechanism of HCSs

3.3.1. OMMT promoting the dispersion of Co_3O_4 in the mixed plastics

To elucidate the roles of OMMT and Co_3O_4 in the formation of the mesoporous HCSs, firstly, polymer/Co_3O_4-10 and polymer/OMMT were pyrolyzed under the same condition. The carbon product from polymer/OMMT was irregular carbon, demonstrating that OMMT was not the real active site for the formation of HCSs. The pyrolysis of polymer/Co_3O_4-10 also led to the formation of HCSs, indicating that Co_3O_4 catalyst was the real active site for the growth of HCSs (Fig. 10) [36]. However, the diameter of HCSs from polymer/Co_3O_4-10 was in the range of 80–160 nm, obviously larger than that from polymer/OMMT-Co_3O_4-10 (i.e., HCS-10, 44–57 nm). This was possibly because that OMMT promoted the dispersion of Co_3O_4 catalyst into small size in the mixed plastics.

To confirm the above speculation, the dispersion states of Co_3O_4 catalyst in the mixed plastics with or without the addition of OMMT are shown in Fig. 11. PS was immiscible with PP and PE, and existed in the form of microspheres (Fig. 11a). OMMT were dispersed in PP and PE matrix (Fig. 11b). Without the addition of OMMT, Co_3O_4 catalyst with a size range of 100–400 nm was agglomerated in PP and PE matrix (Fig. 11c). Interestingly, after the addition of OMMT, the dispersion degree of Co_3O_4 catalyst (Fig. 11d) was significantly higher than that without OMMT. Especially, the size of Co_3O_4 catalyst in the presence of OMMT was evidently smaller (50–100 nm) than that in the case without OMMT. There are two possible reasons for the above phenomenon. One of them results from the viscosity increase of the mixed plastics due to the presence of dispersed OMMT (Fig. 12), which increases shear force during melt mixing and improves the dispersion degree of Co_3O_4 catalyst in the mixed plastics. The other is possible interaction between OMMT and Co_3O_4 catalyst, which prevents the re-aggregation of Co_3O_4 catalyst.

To further verify the effect of OMMT on the formation of HCSs with controllable diameter, the morphologies of carbonized products from polymer/OMMT-Co_3O_4-x and polymer/Co_3O_4-x were compared by TEM observations (Fig. 13). Clearly, when the content of Co_3O_4 was low (e.g., 10 g/100 g polymer), the resultant Co@C core/shell sphere from polymer/Co_3O_4-OMMT-x was in the range of 40–60 nm (Fig. 13a), much smaller than that from polymer/Co_3O_4-x (80–160 nm) (Fig. 13b). This demonstrated that the addition of OMMT promoted the formation of Co@C core/shell sphere with smaller size, which resulted from the smaller size of Co_3O_4 catalyst in the mixed plastics. When the content of Co_3O_4 catalyst increased (e.g., 30 g/100 g polymer), the Co@C core/shell sphere from polymer/Co_3O_4-OMMT-x became larger

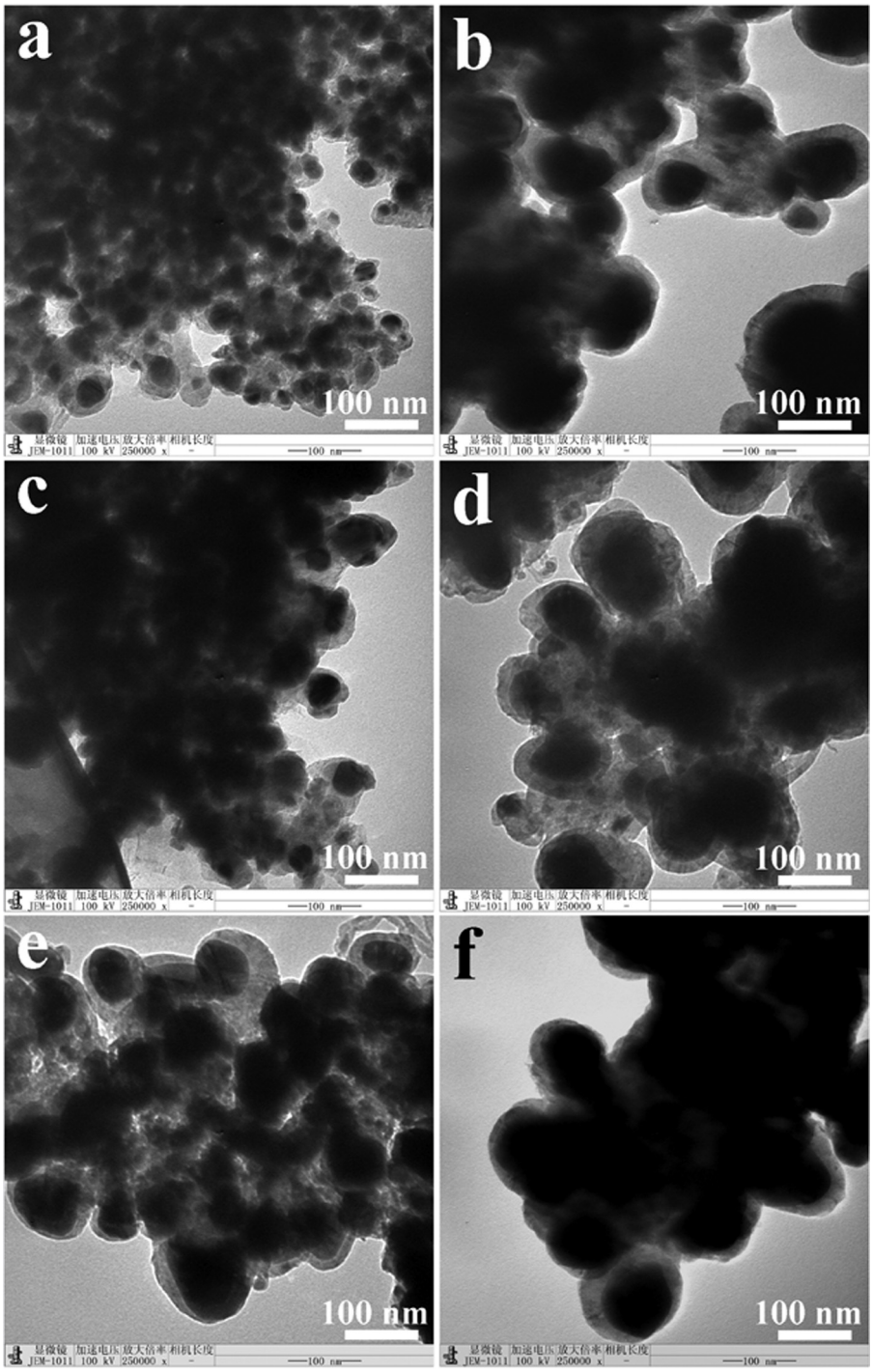

Fig. 13. TEM images of the carbonized products from polymer/OMMT-Co_3O_4-x before purification (Co@C-10 (a), Co@C-30 (c) and Co@C-60 (e)) and polymer/Co_3O_4-x before purification (Co@C-10′ (b), Co@C-30′ (d) and Co@C-60′ (f)).

(Fig. 13c). After further increasing the content of Co_3O_4 catalyst (e.g., 60 g/100 g polymer), the Co@C core/shell sphere from polymer/Co_3O_4-OMMT-x (Fig. 13e) was similar with that from polymer/Co_3O_4-x (Fig. 13f). This was because, after further increasing Co_3O_4 catalyst content, the aggregation of Co_3O_4 catalyst was inevitable. Besides, the average sizes of Co particles in Co@C core/shell spheres from polymer/Co_3O_4-OMMT-x were 40 nm for Co@C-10, 49 nm for Co@C-20, 52 nm for Co@C-30, 63 nm for Co@C-40, 74 nm for Co@C-50, and 89 nm for Co@C-60. Furthermore, in the cases without OMMT, the diameter of Co@C core/shell spheres from polymer/Co_3O_4-x showed no obvious changes (Fig. 13b, d and f). Based on the above results, it was demonstrated that the size of Co@C core/shell spheres could be controlled by the addition of OMMT, which favored to synthesize HCSs with controllable diameter.

3.3.2. *OMMT affecting the degradation products of mixed plastics*

The degradation products of mixed plastics are carbon feedstock for the formation of mesoporous HCSs. To study the influence of OMMT on the degradation products of mixed plastics, GC and GC–MS measurements were conducted to analyze the composition of the degradation products from polymer (i.e., mixed plastics) and

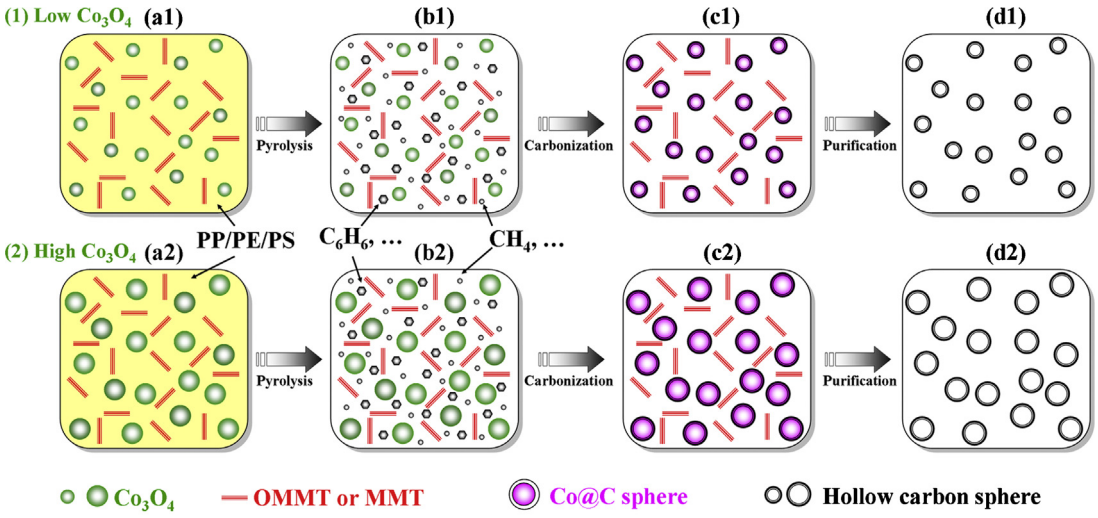

Fig. 14. Possible mechanism about the conversion of mixed plastics (PP, PE and PS) into uniform HCSs with controllable diameter under the combined catalysis of OMMT/Co_3O_4 at 700 °C.

Table 2
Yields of the different fractions through the pyrolysis of polymer (i.e., mixed plastics) and polymer/OMMT at 700 °C.

Product	Polymer	Polymer/OMMT
Carbon (g/100 g polymer)	0.0	1.0
Liquid (g/100 g polymer)	64.2	59.6
Gas (g/100 g polymer)[a]	35.8	39.4

[a] Calculated by the mass balance.

polymer/OMMT at 700 °C. Table 2 presents the mass balance of the degradation products from mixed plastics and polymer/OMMT. After adding 15 (g/100 g polymer) OMMT, the quantity of gas degradation products increased from 35.8 to 39.4 (g/100 g polymer), indicating that OMMT promoted the degradation of mixed plastics into light hydrocarbons. Fig. S3 shows the composition of gas degradation products in detail, which mainly consisted of hydrogen, methane, ethane, ethylene, propane, propylene and *i*-butene. Compared to mixed plastics, the yields of methane, ethylene and propylene from polymer/OMMT increased. For example, the yield of methane increased from 50 to 97.5 (mL/100 g polymer).

Fig. S4 displays the GC–MS profiles of liquid degradation products from mixed plastics and polymer/OMMT. The main liquid degradation products from mixed plastics were olefins with short and long chains, and aromatics including benzene, toluene and ethyl-benzene. After adding OMMT, the content of aromatics significantly increased, meanwhile the olefins with long chains disappeared. The above results demonstrated that OMMT promoted the degradation of mixed plastics into light hydrocarbons and aromatics, which are widely used as carbon sources for the synthesis of carbon spheres [40,41].

Based on the above results and some previous reports [25,26,36], a possible mechanism about the formation of uniform HCSs with controllable diameter through catalytic carbonization of mixed plastics (PP, PE and PS) under the combined catalysis of OMMT/Co_3O_4 was put forward (Fig. 14). When the content of Co_3O_4 was low, OMMT firstly promoted the dispersion of Co_3O_4 catalyst in the mixed plastics (a1); subsequently, OMMT promoted the degradation of mixed plastics into light hydrocarbons and aromatics (b1). Secondly, the resultant light hydrocarbons and aromatics were dehydrogenated and aromatizated on the surface of Co_3O_4 catalyst [36], meanwhile Co_3O_4 catalyst was reduced into metallic cobalt catalyst, which have some (about 1 at%) carbon solubility in the solid solution [42]. After further carbonization of the degradation products, once supersaturated, carbon precipitated from the surface of metallic cobalt nanoparticles to form Co@C core/shell spheres (c1). Obviously, the formation of Co@C core/shell spheres played an important role in the synthesis of mesoporous HCSs with controllable diameter, and the metallic cobalt nanoparticles from the reduction of Co_3O_4 catalyst actually acted as templates for the growth of HCSs. Finally, after the removals of metallic cobalt catalyst and MMT, the mesoporous HCSs with smaller diameter were obtained (d1). When the content of Co_3O_4 was increased, Co_3O_4 catalyst was aggregated inevitably into larger particles (a2). As a result, after the pyrolysis and carbonization (b2), the resultant Co@C core/shell spheres became larger (c2), which promoted the formation of HCSs with larger size after the purification (d2). Finally, the mesoporous HCSs with controllable diameter were prepared effectively through catalytic carbonization of mixed plastics under the combined catalysis of OMMT/Co_3O_4.

4. Conclusion

A simple approach was demonstrated to effectively convert the mixed plastics (PP, PE and PS) into uniform mesoporous HCSs with controllable diameter under the combined catalysis of OMMT/Co_3O_4 at 700 °C. When the content of Co_3O_4 was increased from 10 to 60 (g/100 g polymer), the diameter of HCSs increased from 48.7 to 96.1 nm, and the yield increased from 16.1 to 49.0 wt%. In addition, HCSs had high degree of graphitization, high purity and some surface functional groups such as C–OH, C=O and COOH. The total surface areas and pore volumes of HCSs were in the range of 196–238.7 m^2/g and 0.511–0.753 cm^3/g, respectively. The size of mesopores in the HCSs was in the narrow range of 2–5 nm. Furthermore, OMMT not only promoted the dispersion of Co_3O_4 in the mixed plastics, which favored to control the diameter of HCSs, but also promoted the degradation of mixed plastics into light hydrocarbons and aromatics, which facilitated the growth of HCSs. At last, a possible growth mechanism of mesoporous HCSs with controllable diameter using mixed plastics as carbon sources under the combined catalysis of OMMT/Co_3O_4 was proposed. This facile approach offers a new potential way to transform waste plastics into valuable HCSs, which may be used as catalyst support, adsorbent, storage medium and template for synthesis of other useful hollow materials, etc. The related work is on the way in our laboratory.

Acknowledgements

This work was supported by the National Natural Science Foundation of China (51373171, 2124079, 50873099 and 20804045) and Polish Foundation (No. 2011/03/D/ST5/06119).

Appendix A. Supplementary data

Supplementary material related to this article can be found, in the online version, at http://dx.doi.org/10.1016/j.apcatb.2014.01.051.

References

[1] P.T. Williams, E. Slaney, Resour. Conserv. Recycl. 51 (2007) 754–769.
[2] S.M. Al-Salem, P. Lettieri, J. Baeyens, Waste Manage. 29 (2009) 2625–2643.
[3] D.P. Serrano, J. Aguado, J.M. Escola, ACS Catal. 2 (2012) 1924–1941.
[4] C.F. Wu, P.T. Williams, Appl. Catal. B: Environ. 90 (2009) 147–156.
[5] C.F. Wu, P.T. Williams, Appl. Catal. B: Environ. 87 (2009) 152–161.
[6] J.M. Escola, J. Aguado, D.P. Serrano, A. García, A. Peral, L. Briones, R. Calvo, E. Fernandez, Appl. Catal. B: Environ. 106 (2011) 405–415.
[7] R. Soheilian, A. Davies, S.T. Anaraki, C.W. Zhuo, Y.A. Levendis, Energy Fuel 27 (2013) 4859–4868.
[8] C.F. Wu, Z.C. Wang, L.Z. Wang, P.T. Williams, J. Huang, RSC Adv. 2 (2012) 4045–4047.
[9] C.F. Wu, M.A. Nahil, N. Miskolczi, J. Huang, P.T. Williams, Environ. Sci. Technol. 48 (2014) 819–826.
[10] J.C. Acomb, C.F. Wu, P.T. Williams, Appl. Catal. B: Environ. 147 (2014) 571–584.
[11] C.W. Zhuo, B. Hall, H. Richter, Y. Levendis, Carbon 48 (2010) 4024–4034.
[12] C.W. Zhuo, J.O. Alves, J.A.S. Tenorio, Y.A. Levendis, Ind. Eng. Chem. Res. 51 (2012) 2922–2930.
[13] C.W. Zhuo, Y.A. Levendis, J. Appl. Polym. Sci. 131 (2014) 39931–39944.
[14] V.G. Pol, M.M. Thackeray, Energy Environ. Sci. 4 (2011) 1904–1912.
[15] T. Tang, X.C. Chen, X.Y. Meng, H. Chen, Y.P. Ding, Angew. Chem. Int. Ed. 44 (2005) 1517–1520.
[16] Z.W. Jiang, R.J. Song, W.G. Bi, J. Lu, T. Tang, Carbon 45 (2007) 449–458.
[17] R.J. Song, Z.W. Jiang, W.G. Bi, W.X. Cheng, J. Lu, B.T. Huang, T. Tang, Chem. Eur. J. 13 (2007) 3234–3240.
[18] J. Gong, J. Liu, Z.W. Jiang, X. Wen, X.C. Chen, E. Mijowska, Y.H. Wang, T. Tang, Chem. Eng. J. 225 (2013) 798–808.
[19] J. Gong, J.D. Feng, J. Liu, R. Muhammad, X.C. Chen, Z.W. Jiang, E. Mijowska, X. Wen, T. Tang, Ind. Eng. Chem. Res. 52 (2013) 15578–15588.
[20] J. Gong, J. Liu, L. Ma, X. Wen, X.C. Chen, D. Wan, H.O. Yu, Z.W. Jiang, E. Borowiak-Palen, T. Tang, Appl. Catal. B: Environ. 117–118 (2012) 185–193.
[21] J. Gong, K. Yao, J. Liu, X. Wen, X.C. Chen, Z.W. Jiang, E. Mijowska, T. Tang, Chem. Eng. J. 215–216 (2013) 339–347.
[22] J. Gong, J. Liu, Z.W. Jiang, J.D. Feng, X.C. Chen, L. Wang, E. Mijowska, X. Wen, T. Tang, Appl. Catal. B: Environ. 147 (2014) 592–601.
[23] J. Gong, J. Liu, D. Wan, X.C. Chen, X. Wen, E. Mijowska, Z.W. Jiang, Y.H. Wang, T. Tang, Appl. Catal. A: Gen. 449 (2012) 112–120.
[24] C.F. Wu, P.T. Williams, Fuel 89 (2010) 3022–3032.
[25] A. Nieto-Márquez, R. Romero, A. Romero, J. Valverde, J. Mater. Chem. 21 (2011) 1664–1672.
[26] A.A. Deshmukh, S.D. Mhlanga, N.J. Coville, Mater. Sci. Eng. R 70 (2010) 1–28.
[27] F.D. Han, Y.J. Bai, R. Liu, B. Yao, Y.X. Qi, N. Lun, J.X. Zhang, Adv. Energy Mater. 1 (2011) 798–801.
[28] K. Tang, L.J. Fu, R.J. White, L.H. Yu, M.-M. Titirici, M. Antonietti, J. Maier, Adv. Energy Mater. 2 (2012) 873–877.
[29] J.H. Kim, B.Z. Fang, S.B. Yoon, J.-S. Yu, Appl. Catal. B: Environ. 88 (2009) 368–375.
[30] G.D. Li, C.L. Guo, C.H. Sun, Z.C. Ju, L.S. Yang, L.Q. Xu, Y.T. Qian, J. Phys. Chem. C 112 (2008) 1896–1900.
[31] W. Konicki, K. Cendrowski, X.C. Chen, E. Mijowska, Chem. Eng. J. 228 (2013) 824–833.
[32] X.C. Chen, K. Kierzek, Z.W. Jiang, H.M. Chen, T. Tang, M. Wojtoniszak, R.J. Kalenczuk, P.K. Chu, E. Borowiak-Palen, J. Phys. Chem. C 115 (2011) 17717–17724.
[33] X.C. Chen, K. Kierzek, K. Wilgosz, J. Machnikowski, J. Gong, J.D. Feng, T. Tang, R.J. Kalenczuk, H.M. Chen, P.K. Chu, E. Mijowska, J. Power Sources 216 (2012) 475–481.
[34] X.C. Chen, K. Kierzek, K. Wenelska, K. Cendrowski, J. Gong, X. Wen, T. Tang, P.K. Chu, E. Mijowska, Chem. Asian J. 8 (2013) 2627–2633.
[35] X.C. Chen, H. Wang, J.H. He, Nanotechnology 19 (2008) 325607.
[36] J. Gong, J. Liu, X.C. Chen, X. Wen, Z.W. Jiang, E. Mijowska, Y.H. Wang, T. Tang, Micropor. Mesopor. Mater. 176 (2013) 31–40.
[37] J.O. Alves, C.W. Zhuo, Y.A. Levendis, J.A.S. Tenório, Appl. Catal. B: Environ. 106 (2011) 433–444.
[38] R. Demir-Cakan, N. Baccile, M. Antonietti, M.-M. Titirici, Chem. Mater. 21 (2009) 484–490.
[39] X.H. Song, Y.B. Wang, K.A. Wang, R. Xu, Ind. Eng. Chem. Res. 51 (2012) 13438–13444.
[40] Y.Z. Jin, C. Gao, W.K. Hsu, Y.Q. Zhu, A. Huczko, M. Bystrzejewski, M. Roe, C.Y. Lee, S. Acquah, H. Kroto, D.R.M. Walton, Carbon 43 (2005) 1944–1953.
[41] V.G. Pol, M. Motiei, A. Gedanken, J. Calderon-Moreno, M. Yoshimura, Carbon 42 (2004) 111–116.
[42] C.P. Deck, K. Vecchio, Carbon 44 (2006) 267–275.